Impact of Interstitial Mass Transport Resistance on Water Vapor Diffusion Through Fabric Layers

Anshul Sharma
Department of Mechanical Engineering,
University of Texas,
Austin, TX 78712

Sandra K. S. Boetcher
Department of Mechanical Engineering,
Embry-Riddle Aeronautical University,
Daytona Beach, FL 32114

Walid A. Aissa
Department of Mechanical Power,
High Institute of Energy,
South Valley University,
Aswan, Egypt 81528

Matthew J. Traum
Department of Mechanical Engineering,
Milwaukee School of Engineering,
Milwaukee, WI 53202

Textiles maintain wearer comfort by allowing evaporated sweat to permeate through, providing thermal management and keeping skin dry. For single layers, resistance to mass transport is relatively straightforward. However, when textiles are layered, water vapor transport becomes more complex because diffusing molecules must traverse interstitial spaces between layers. Interstitial mass transport resistances of significant magnitude can reduce rates of water vapor transport through layered textile stacks. The prevailing textile mass transport resistance interrogation method is ASTM F1868: "Standard Test Method for Thermal and Evaporative Resistance of Clothing Materials Using a Sweating Hot Plate." Four improvements to ASTM F1868 are recommended: (1) gravimetric mass transport measurement, (2) evaluating transport using the Stefan flow model, (3) correct accounting for apparatus mass transport resistances, and (4) recognizing and measuring interstitial mass transport resistances. These improvements were implemented and evaluated by running tests using Southern Mills Defender™ 750 fabric, the calibration standard used for ASTM F1868, on a new gravimetric experimental apparatus. For a single layer of calibration fabric, the gravimetric approach is consistent with the prescribed result from ASTM F1868; however, for stacks of two or more calibration fabric layers, the gravimetric approach does not agree with the prescribed ASTM F1868 result due to interstitial mass transport resistance between fabric layers. [DOI: 10.1115/1.4005733]

Introduction

Human comfort depends upon the heat and mass transport properties of layered textiles. In cold environments, layered clothing provides thermal insulation to keep the wearer warm while fabric wicks and diffuses away sweat, keeping the skin dry. In hot environments, clothing layers provide protection from direct sunlight while allowing sweat to evaporate from the skin to carry energy bound as latent heat away from the wearer, enabling homeostatic thermal management. Regardless of whether the environment is hot, cold, dry, or humid, properly designed outfits must provide the right balance of heat and mass transport to keep the wearer comfortable and dry. Clothing that fails to allow sweat to evaporate and pass through to the environment leaves the wearer wet and uncomfortable.

Most clothing is made from woven fabric, which contains periodically distributed air-filled pores. These pores are the natural voids between interwoven threads (Fig. 1), and they promote water vapor mass transport. Compared to the slow transport that might occur though the fabric's solid phase (i.e., the thread), these pores provide a low-resistance diffusion path for water vapor through the fabric. If the pores were not present, water vapor could not easily permeate. Porous fabric, therefore, presents a low but non-negligible mass transport resistance to water vapor. In parlance of the Ohm's Law circuit analogy, a mass flux of water vapor is driven across the fabric (akin to current in Ohm's Law) by a chemical concentration gradient (akin to voltage in Ohm's Law) and fabric layers present mass transport resistances (akin to electrical resistances in Ohm's Law). Understanding the underlying heat and mass transport phenomena arising during these transport processes is critical to a range human comfort and protection applications from military and first-responder gear to high-performance athletic apparel.

The prevailing standard method to measure heat and mass transfer resistances in fabrics and predict resulting human comfort parameters is ASTM F1868: "Standard Test Method for Thermal and Evaporative Resistance of Clothing Materials Using a Sweating Hot Plate" [1]. The calibration procedure for ASTM F1868 first measures the parasitic mass transport resistance of the experimental apparatus. Then progressive layers of Southern Mills Defender™ 750 calibration fabric are added (four being the maximum) to the sweating hot plate to provide successively increasing mass transport resistances. The standard gives 0.0172 kPa m^2/W with a $\pm$ 10% allowance as the required resistance for four calibration fabric layers. The standard also prescribes a linear slope of 0.0043 kPa m^2/W per layer of fabric subtracted from the stack. Moreover, ASTM F1868 allows the calibration result to deviate by up to 10% from the stated value, e.g., up to 0.00043 kPa m^2/W per layer of Southern Mills Defender™ 750 calibration fabric in the fabric stack being tested.

In this paper, we suggest four improvements that will enhance the consistency and accuracy of an ASTM F1868-type test: (1) gravimetric mass transport measurement, (2) incorporating Stefan flow into the transport model, (3) accounting correctly for parasitic apparatus mass transport resistances, and (4) recognizing and measuring interstitial layer mass transport resistances. By implementing these improvements, we have created a new *gravimetric* fabric heat and mass transport interrogation method that returns a true, intrinsic, mass transport resistance for the fabric being tested that is fit for use in engineering design of textile systems. While this approach shares some similarities to ASTM F1868, its key difference is direct gravimetric measurement of mass evaporating through the fabric stack. This method juxtaposes existing calorimetric or psychometric approaches, which give indirect indications of mass transport based on temperature and/or humidity measurements. Using the experiment here described, one, two,

Manuscript received June 5, 2011; final manuscript received December 10, 2011; published online October 12, 2012. Assoc. Editor: S. A. Sherif.

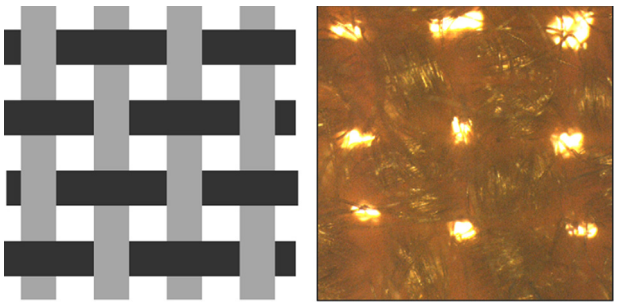

Fig. 1 Textiles are made from repeating woven thread patters (left), which produce void spaces (right). These voids act as pores that readily conduit evaporated water vapor through fabrics.

three, and four layers of Southern Mills Defender™ 750 calibration fabric were tested and the results are compared to ASTM F1868. Furthermore, this paper reports measurements of the mass transport resistance presented by the interstitial space between these calibration fabric layers.

Background and Motivation

Numerous heat and mass transport interrogation methods that simulate sweating human skin in contact with fabric are available [2]. For example, the dynamic moisture permeation cell (DMPC) [3], a psychometric measurement approach, yields mass transfer resistances for fabrics using measured changes in water vapor concentration between two gas streams of controlled temperature and humidity passing across either side of a fabric barrier. This technique has also been successfully applied to testing electrospun mats, which are a type of nonwoven porous barrier [4]. A recently introduced interrogation technique, which is also a psychometric measurement approach, combines elements of DMPC and ASTM F1868 by testing vapor permeability of fabric samples separated from a liquid water reservoir by a thin polytetrafluoroethylene membrane to more realistically simulate human skin [5,6]. Nonetheless, ASTM F1868 is still the most established and preferred standard for human comfort testing of fabrics.

McCullough et al. [7] correlated five of the most prominent standard methods, including ASTM F1868, to each other by measuring and comparing evaporative resistance of 26 different breathable shell fabrics using each testing method. They concluded that the mass transport resistances of the ASTM F1868-type sweating hot plate tests vary less with changes in test conditions than the other methods. ASTM F1868 is also attractive for its close simulation of the heat and mass transfer conditions presented by human skin/clothing systems [8].

The guarded sweating hot plate is an indirect calorimetric method to evaluate resistance to mass transport, R_{ASTM}, presented by a fabric stack. Equation (1) is used to calculate this resistance,

$$R_{\mathrm{ASTM}} = \frac{P_{A,1} - P_{A,2}}{\dot{Q}''} \tag{1}$$

where $P_{A,i}$ is the partial pressure of species A (e.g., water vapor) at station i (station 1 is upstream and station 2 is downstream of the fabric with respect to the water vapor diffusion direction) and $\dot{Q}''$ is the heat flux through the hot plate.

Ideal ASTM F1868 test conditions recommend $\dot{Q}''$ be set to fix the temperature on either side of the fabric stack at 308.15 K (35 °C). Setting upstream and downstream temperatures fixes P_2 and P_1. The station 2 humidity, 40%, is established by placing the entire experiment in an environmental chamber and directing temperature- and humidity-controlled air at 1 m/s over the fabric stack [9]. The upstream relative humidity at station 1, 100%, is established by a continuously replenished liquid water film on the hot plate. Despite simulating sweat evaporation, ASTM F1868 uses distilled, de-ionized, or reverse osmosis-treated water (not brackish water) to avoid the apparatus fouling due to residues left after evaporation. Water entering the hot plate is preheated to 308.15 K by passing through the guard heater, and the fabric is kept dry by a porous hydrophobic membrane placed between the sweating hot plate and the fabric. Maintaining both sides of the fabric stack at 308.15 K eliminates any heat transfer through the fabric stack by conduction (although a correction is built into the standard should achieving isothermal conditions prove impossible). Therefore, the measured hot plate heat flux, $\dot{Q}''$, required to achieve prescribed test conditions establishes mass transport resistance indirectly via Eq. (1), but mass transport itself is not directly measured.

Equation (1) is valid provided the transport through the fabric stack occurs by pure Fickian diffusion. The assumption of Fickian diffusion is appropriate only for (1) barriers whose pores present a Knudsen number, Kn, much less than one and (2) mixtures of water vapor and air that are very dilute.

With respect to high-Knudsen-number rarefaction effects, an earlier version of the new gravimetric apparatus described here measured evaporative cooling via vapor transport through two different microtruss-like barriers with pores of 15 μm and 1 μm, respectively. Under ambient pressure and temperature conditions, rarefaction effects were not observed for barriers with pore diameters as small as 1 μm (Kn $\sim$ 0.1) within the uncertainty of the experiment ($\pm$ 12%) [10]. Indeed, this result is consistent with *transition diffusion regime theory*, which predicts retardation from the bulk diffusion coefficient of only 11.4% for 1 μm (Kn $\sim$ 0.1) pores under ambient pressure and temperature conditions. Since the pores in the calibration fabric barriers studied in this current effort are on average about 200 μm (Kn $\sim$ 0.003) in characteristic diameter (Fig. 2), the expected retardation in diffusion coefficient is less than 0.52% owing to rarefaction. Thus, for this analysis the slight rarefaction effect of Southern Mills Defender™ 750 fabric caused by small pore diameter will be ignored. We assume, therefore, that diffusion processes studied here are not functions of pore diameter.

With respect to flow enhancements caused by nondilute water vapor air mixtures, the so-called *Stefan flow* (convection caused by diffusion) produces a mass flux enhancement of 3.9% beyond pure Fickian diffusion for ASTM F1868 conditions, as described below. While a 3.9% effect could likely be ignored in most engineering analyses, ASTM F1868 demands experimental precision within at least $\pm$10% of tabulated calibration fabric values, and the 3.9% Stefan flow enhancement is an appreciable fraction of the required level of precision. So, this enhancement effect cannot be ignored as it is by the ASTM F1868 model of Eq. (1).

Additionally, the intrinsic fabric barrier mass transport resistance must be isolated from the parasitic resistance induced by the apparatus by forced convection on the fabric's downstream face. In a related series of evaporative cooling experiments, Johnson

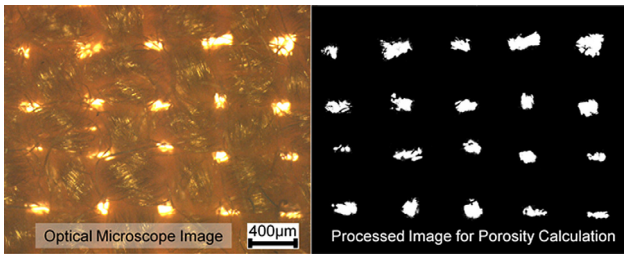

Fig. 2 Twenty optical micrographs captured the fine pore structure of a Southern Mills Defender™ 750 calibration fabric sample (similar to the left image). The resulting images were then each manually postprocessed using NIH ImageJ to isolate the pores. Porosity (with standard deviation) for the fabric was calculated using the white/black pixel ratio of the processed images.

et al. [11] established the importance of calculating or measuring boundary layer mass transfer resistances on the outside surfaces porous barriers and demonstrated that these resistances can dominate transport processes, especially when a barrier's mass transport resistance is relatively small in relation. The ASTM F1868 protocol includes an initial test of the bare membrane-covered sweating hot plate without fabric to establish the apparatus-induced convective mass transport resistance. An apparent ASTM F1868 inconsistency arises in the way the linear slope of fabric-stack resistance versus number of fabric layers is extrapolated back to zero layers. With zero fabric layers in place, the total measured mass transport resistance should equal the parasitic apparatus mass transport resistance due to forced convection. Instead, however, the prescribed value is zero.

A second apparent ASTM F1868 inconsistency is the linearity of the stack resistance versus number of fabric layers slope from zero to two layers and two to four layers of calibration fabric (four layers being the maximum tested during calibration). The prescribed constant slope omits interstitial mass transport resistances that arise, akin to contact resistances in heat transfer, when fabrics are layered atop each other. Thus, the slope from $0 \leq N < 2$ should be different than the slope for $2 \leq N \leq 4$ (where N is the number of fabric layers) because when multiple fabric layers are present, interstitial spaces with their own mass transport resistances are formed. In addition to the resistances induced by interstitial air gap between fabric layers, layering also induces tortuosity owing to pore misalignment between fabric layers, further increasing transport resistance—see Fig. 3. These phenomena together increase overall mass transport resistance of a stack of layered fabrics beyond the value expected by sum of individual resistances of the component layers.

To eliminate some of these inconsistencies, a heat and mass transport apparatus, which gravimetrically measures mass transport through porous barriers, including fabric stacks, was used to measure the mass transport resistance (including interstitial transport resistance) presented by one, two, three, and four Southern Mills Defender^{TM} 750 calibration fabric layers to provide comparison against ASTM F1868. These results are reported here. This apparatus has already been successfully used to measure the rates of water vapor transport through a series of track-etched polycarbonate barriers ($\sim$25 μm thick) with a range of nanometer-diameter through pores from 39 nm to 5400 nm. That experiment produced results in good agreement with the transition diffusion regime model after a correction factor to account for pore tortuosity was applied [12].

Analytical Approach

Water vapor transport through porous barriers owing to a concentration gradient for which the vapor component is too high to be considered "dilute" is best described by the Stefan flow model.

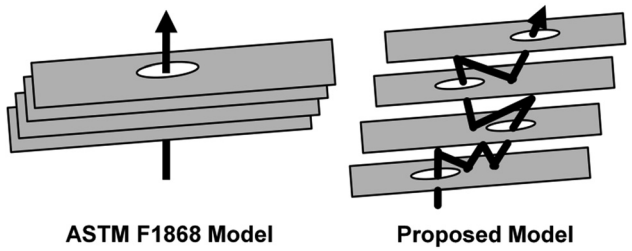

Fig. 3 The ASTM F1868 testing protocol assumes a linear relationship between number of fabric layers and total resistance to mass transport presented by a fabric stack, which implies that resistances to mass transport in the interstitial spaces between fabric layers are inconsequential. Testing layered ASTM calibration fabrics using a gravimetric technique shows that interstitial air gaps and tortuosity are nontrivial mass transport resistance components of fabric stacks.

This model is derived from first principles by considering the one-dimensional transit of ideal gas species A against a stationary background of ideal gas species B confined into a right cylindrical pore under a concentration gradient of species A [13]. The total mass flux of species A per unit area through one pore, $\dot{m}''_{A,\text{pore}}$, is the sum of the bulk diffusion and convection processes happening in parallel

$$\dot{m}''_{A,\text{pore}} = -D_{A,B}\rho\frac{dy_A}{dz} + y_A\dot{m}''_{A,\text{pore}} \tag{2}$$

where $D_{A,B}$ is the bulk diffusion coefficient of species A in B, y_A is the mole fraction of species A, z is the spatial coordinate system along which transport occurs, and ρ is the total concentration (by mass) of both species A and B combined. If species A is dilute (i.e., $y_A \approx 0$), Eq. (2) is approximated by the familiar expression for Fickian diffusion

$$\dot{m}''_{A,\text{pore}} = -D_{A,B}\rho\frac{dy_A}{dz} \tag{3}$$

or the integrated form

$$\dot{m}''_{A,\text{pore}} = \frac{-D_{A,B}}{L}\left(\rho_{A,2} - \rho_{A,1}\right) \tag{4}$$

where $\rho_{A,1}$ and $\rho_{A,2}$ are the concentration (by mass) of species A an stations 1 and 2, respectively, and L is the thickness of the barrier the vapor is traversing. Note that Eq. (4) describes the vapor transport process for a single pore. To model the combined effect of all pores inlayed within a porous barrier, the barrier's porosity ε and area A must be considered. It is also typical to include a fitting parameter called tortuosity τ which accounts for deviations in pore geometry from the perfect, right cylinders assumed in the original derivation. Thus, for Fickian diffusion, the mass transfer through a porous barrier is written as

$$\dot{m}''_{A} = \frac{-A\varepsilon D_{A,B}}{\tau L}\left(\rho_{A,2} - \rho_{A,1}\right) \tag{5}$$

Invoking the Ohm's Law analogy for mass transfer, the coefficient terms preceding the concentration difference are collected into a mass transport resistance to yield the following expression:

$$\dot{m}_A = \frac{-A}{R_{\text{barrier}}}\left(\rho_{A,2} - \rho_{A,1}\right) \tag{6a}$$

where

$$R_{\text{barrier}} = \frac{\tau L}{\varepsilon D_{A,B}} \tag{6b}$$

which is competent for combination with other mass transport resistances (i.e., the convection mass transport resistance on the downstream barrier face in ASTM F1868 owing to air forced over that surface) to model mass transfer processes using the Ohm's Law analogy.

However, in the case when species A is not dilute (i.e., $y_A > 0$), the term on the far right hand side of Eq. (2) cannot be neglected, and the expression becomes

$$\dot{m}''_{A,\text{pore}}(1 - y_A) = -D_{A,B}\rho\frac{dy_A}{dz} \tag{7}$$

or the integrated form

$$\dot{m}''_{A,\text{pore}} = \frac{D_{A,B}\rho}{L}\ln\left[\frac{1 - y_{A,2}}{1 - y_{A,1}}\right] \tag{8}$$

where $y_{A,1}$ and $y_{A,2}$ are the mole fractions of species A at stations 1 and 2, respectively. As it was already assumed that both the

diffusing species and the background species behave as ideal gasses, $y_{A,i}$ is better expressed in terms of partial pressures to put the entire expression in terms of familiar thermodynamic variables.

$$\dot{m}''_{A,\text{pore}} = \frac{D_{A,B}\rho}{L}\ln\left[\frac{1-\frac{P_{A,2}}{P_2}}{1-\frac{P_{A,1}}{P_1}}\right] \tag{9}$$

As with Fickian diffusion, this Stefan flow expression for a single pore can be applied to an entire porous barrier and the mass transport resistance of the barrier expressed as an Ohm's Law equivalent resistance to facilitate mass transfer process modeling

$$\dot{m}_A = \frac{A}{R_{\text{barrier}}}\rho\ln\left[\frac{1-\frac{P_{A,2}}{P_2}}{1-\frac{P_{A,1}}{P_1}}\right] \tag{10a}$$

where

$$R_{\text{barrier}} = \frac{\tau L}{\varepsilon D_{A,B}} \tag{10b}$$

Note that the expressions for mass transfer resistance arising from Fickian diffusion and Stefan flow are identical and the only difference between these two approaches is how the concentration gradient potential driving the transport process is calculated. To estimate the percentage difference between Fickian diffusion and Stefan flow for conditions typical of ASTM F1868, the following ratio is calculated:

$$\frac{\dot{m}_{A,\text{Stefan}}}{\dot{m}_{A,\text{Fick}}} = \frac{\frac{A}{R_{\text{barrier}}}\rho\ln\left[\frac{1-\frac{P_{A,2}}{P_2}}{1-\frac{P_{A,1}}{P_1}}\right]}{\frac{-A}{R_{\text{barrier}}}\left(\rho_{A,2}-\rho_{A,1}\right)} \tag{11a}$$

$$\frac{\dot{m}_{A,\text{Stefan}}}{\dot{m}_{A,\text{Fick}}} = \frac{-\ln\left[\frac{1-\frac{P_{A,2}}{P_2}}{1-\frac{P_{A,1}}{P_1}}\right]}{\left(\frac{\rho_{A,2}-\rho_{A,1}}{\rho}\right)} \tag{11b}$$

$$\frac{\dot{m}_{A,\text{Stefan}}}{\dot{m}_{A,\text{Fick}}} = \frac{-\ln\left[\frac{1-\frac{P_{A,2}}{P_2}}{1-\frac{P_{A,1}}{P_1}}\right]}{\left(\frac{P_{A,2}}{P_2}-\frac{P_{A,1}}{P_1}\right)} \tag{11c}$$

The ASTM test occurs in an environmental chamber where at the downstream station $P_2 = 103576.2$ Pa, $T_2 = 308.15$ K, and $\text{RH}_2 = 40\%$. Note that the slight elevation above normal atmospheric pressure is due to the added partial pressure of water vapor. These conditions give the partial pressure of water vapor at station 2, $P_{A,2} = 5628$ Pa. At the upstream station, $T_1 = 308.15$ K and $\text{RH}_1 \approx 100\%$ due to the presence of liquid water sitting on the sweating hot plate. The partial pressure of water vapor at station 1, $P_{A,1} = 2251.2$ Pa, and the total pressure at station 1 is atmospheric pressure plus the partial pressure of water vapor, $P_1 = 106953$ Pa.

These values give $P_{A,1}/P_1 = 0.052621$ and $P_{A,2}/P_2 = 0.021735$, which yield a ratio of Stefan to Fickian vapor mass transport of 1.039 per Eq. (11*c*). In other words, by neglecting the Stefan Flow enhancement in the transport process and assuming pure Fickain diffusion, ASTM F1868 attributes a mass flux 3.9% higher than it should be to the mass transport resistance of a sample fabric stack. The resulting measured fabric mass transport resistance appears lower than it actually is. As stated above, this 3.9% increase is small enough that it would likely be ignored in most engineering analyses. However, this unaccounted-for-flow-enhancement is a significant fraction of the ±10% measurement deviation allowed by the ASTM standard.

In this derivation, water vapor is treated as an ideal gas. Under the prescribed conditions ($T = 308.15$ K and $P_A = 5628$ Pa), this assumption is appropriate because the associated compressibility factor for water vapor is 1.002, indicating about 0.2% deviation between the actual properties of water vapor and the ideal gas approximation.

Another issue with the mass transport resistance, R_{ASTM}, obtained using ASTM F1868 is that while its units are technically correct, it is not equivalent to the true Ohms Law analogy mass transfer resistance given in Eq. (6*b*) because it includes embedded thermodynamic properties of the working fluid (e.g., water vapor). To derive the conversion between R_{ASTM} and an Ohms Law competent mass transfer resistance derived from Fickian diffusion, R_{Fick}, consider how these two terms would be calculated for the same water vapor transport process. R_{Fick} is solved from Eq. (6*a*)

$$R_{\text{Fick}} = \frac{\left(\rho_{A,1}-\rho_{A,2}\right)}{\dot{m}''_A} \tag{12}$$

To transform this expression into R_{ASTM} variables, the ideal gas law (where $\bar{R}$ is the gas constant for water vapor) is applied. It is recognized that for ASTM F1868, the temperature on both barrier faces is the same value, T, which gives

$$R_{\text{Fick}} = \frac{\left(\frac{P_{A,1}}{\bar{R}T_{A,1}}-\frac{P_{A,2}}{\bar{R}T_{A,2}}\right)}{\dot{m}''_A} = \frac{\frac{1}{\bar{R}T}\left(P_{A,1}-P_{A,2}\right)}{\dot{m}''_A} \tag{13}$$

To transform the R_{ASTM} expression, Eq. (1) is solved for R_{ASTM} noting that the thermal energy input at the sweating hot plate to maintain steady-state experimental conditions must be the product of mass flux through the barrier and the latent heat of vaporization of water, ΔH_{fg}, at 308.15 K

$$R_{\text{ASTM}} = \frac{\left(P_{A,1}-P_{A,2}\right)}{\dot{m}''_A \Delta H_{fg}} \tag{14}$$

Equations (13) and (14) are both solved for the mass flux per unit area, $\dot{m}''_A$, which must have one value regardless of the mass transfer resistance approach followed. Thus,

$$\frac{\frac{1}{\bar{R}T}\left(P_{A,1}-P_{A,2}\right)}{R_{\text{Fick}}} = \dot{m}''_A = \frac{\left(P_{A,1}-P_{A,2}\right)}{R_{\text{ASTM}}\Delta H_{fg}} \tag{15}$$

Finally, eliminating redundant variables from both sides of Eq. (15) reveals the relationship between R_{Fick} and R_{ASTM} and shows the embedded thermodynamic properties within R_{ASTM}.

$$R_{\text{Fick}}\left(\frac{\bar{R}T}{\Delta H_{fg}}\right) = R_{\text{ASTM}} \tag{16}$$

For water at 308.15 K and 1 atm pressure, $\Delta H_{fg} = 2.418 \times 10^6$ J/kg, and $\bar{R} = 0.4614$ J/kg K. Thus, $R_{\text{Fick}}/R_{\text{ASTM}} = 17.0$. For a single layer of calibration fabric, $R_{\text{ASTM}} = 4.30 \pm 0.43$ s/m (as prescribed in ASTM F1868), while R_{Fick} was measured by our gravimetric apparatus at 60.3 ± 14.4 s/m, giving an expected $R_{\text{Fick}}/R_{\text{ASTM}}$ ratio of 14.0 ± 3.6. The anticipated ratio, 17.0, is within this range, demonstrating the interchangeability of these two approaches (within experimental uncertainty) for evaluating barrier mass transport resistance using ASTM F1868-type experiments.

The working-fluid-property reliance of R_{ASTM} has three major drawbacks. First, measured R_{ASTM} values cannot be applied universally to a range of evaporating working fluids. For example, if R_{ASTM} were known for a particular porous barrier using water vapor, that measured mass transport resistance would not apply to the same barrier for transport of working fluids other than water; alcohols, for instance. On the other hand, mass transport resistance values obtained through the gravimetric method of this paper need only be multiplied by the ratio of diffusion coefficients for water vapor and the new working fluid to remain valid.

Second, since R_{ASTM} contains both fabric physical properties and working-fluid thermodynamic properties, it is not an Ohm's Law equivalent mass transport resistance, and it cannot be used for engineering analysis of mass transport problems. For example, R_{ASTM} is not competent to model one-dimensional mass transport through a porous barrier where there are other known resistances abutting the upstream and downstream barrier faces (i.e., calculated using a Sherwood number correlation). Therefore, R_{ASTM} is most useful as an index to compare the performance of different fabrics, but it cannot be applied within other modeling approaches (i.e., the Ohm's Law analogy) for quantitative engineering design of fabric systems.

Third, since R_{ASTM} includes embedded thermodynamic properties of the working fluid, its value is highly susceptible to variations in fluid properties resulting from variations in state (i.e., temperatures and pressures deviating from prescribed values). For example, the latent heat of vaporization for pure water changes by as much as 1% with a ± 10 K excursion in temperature away from the 308.15 K (35 °C) prescribed by ASTM F1868. Thus, measured R_{ASTM} values are representative only in the immediate temperature range of the ASTM F1868 calibration. Moreover, changes in latent heat of vaporization can occur if even slight amounts of impurities (especially surfactants) get dissolved in the water. Although ASTM F1868 uses fresh water, it simulates evaporation from skin where the sweat is a solution containing salts. Latent heat of vaporization for aqueous saline solutions varies by more than $\pm 1.7\%$ at 30 °C from fresh water values depending on the type and amount of salt dissolved [14]. Moreover, contact between water and the tubing and metal surfaces during the ASTM 1868 test could impart contaminants to the working fluid, change its evaporative properties, and adversely impact the measurement accuracy of R_{ASTM}. Since the gravimetric technique described here does not embed working-fluid thermodynamic properties into the measured barrier mass transport resistance, the proposed technique will provide a repeatable result despite salinity or other dissolved impurities in the water.

Fabric Barrier Characterization. The porosity ε and thickness L of Southern Mills Defender^{TM} 750 were measured to estimate the mass transport resistance of the calibration fabric using Eq. (6*b*) independent of measured experimental values to provide a basis of comparison. The barrier thickness was measured at 65.58 ± 2.54 μm using a micrometer.

Since fabrics are woven, the void spaces between the treads, (e.g., the pores) are observable with an optical microscope at 10× zoom. To calculate porosity, 20 optical micrographs where taken each of unique sections of one fabric layer using a Nikon E600 Eclipse microscope. These digital images were then imported into ImageJ (an image processing and analysis software tool freely available through the National Institutes of Health (NIH)) one at a time and rendered in black and white pixels to isolate the pores in each image. Some manual image processing was also applied to eliminate obvious artifacts like light reflecting off the threads (see Fig. 2 for a sample image from this process). Using ImageJ, the ratio of white to black pixels was calculated for each image, giving the porosity for each micrograph. Statics arising from 20 processed images returned an average porosity 0.054 with a standard deviation in porosity of 0.009.

The validity of using micrograph images to measure barrier porosity when the pores are known to run straight through between external barrier faces (as is the case for these fabrics) was established by Hernandez et al. [15], and the image processing approach used here is similar to that reported by Clavo et al. [16].

Evaporation Experiment. The gravimetric evaporation experiments used to interrogate fabric stacks of Southern Mills Defender^{TM} 750 applied a known, constant heat flux density (400 W/m^2 to match the human metabolic rate) to the underside of a 42-mm-diameter by 2.1-mm-deep pool of de-ionized liquid water in a shallow cylindrical evaporation chamber made of brass (see Fig. 4) sealed at its top with a fabric barrier stack. The evaporation chamber was held in good thermal contact with a Kapton heating element using four nylon screws, which also served as legs to keep the chamber elevated off the balance pan to reduce parasitic conductive heat loss. Power to the heater was supplied by a battery whose output was regulated by a small DC power supply to provide constant power despite slight depletion of the battery voltage during each experiment.

The cumulative weight loss versus time, owing to water evaporation and transport to the environment through the barrier's pores, was measured by continuously monitoring the weight of the entire evaporation experiment using a Mettler-Toledo XS6002S precision balance. Precise gravimetric measurement was enabled by keeping the entire experiment (including batteries to power the heater and all data-logging instruments) atop the

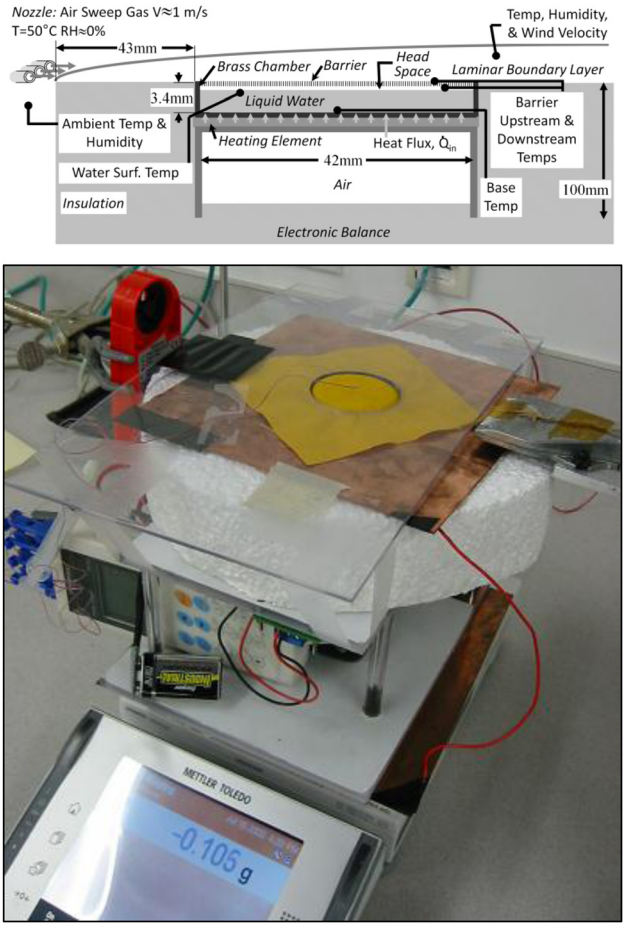

Fig. 4 (Top) A schematic (not to scale) of the evaporation apparatus for measuring resistance to water vapor transport from porous barriers and textiles. Shown are important temperature measurement locations. (Bottom) The apparatus shown running with one layer of Southern Mills Defender^{TM} 750 calibration fabric—the textile material.

scale with no mechanical or electrical connections to the lab bench. The experiment was so sensitive that the mechanical rigidity of wires running between the scale and bench would have created false balance readings.

Assuming mass transfer resistances are series additive (per the Ohm's Law model), the steady-state flux of water vapor through the pores (from Eq. (10*a*)) is

$$\dot{m}_A = \frac{A}{R_{\text{barrier}} + R_{\text{US}} + R_{\text{DS}}} \rho \ln \left[\frac{1 - \frac{P_{A,2}}{P_2}}{1 - \frac{P_{A,1}}{P_1}} \right] \tag{17}$$

where R_{US} and R_{DS} are, respectively, the steady-state resistances to water vapor mass transport in the region between the liquid water surface and the barrier entrance (upstream (US) of fabric barrier stack with respect to the diffusion direction) and across the concentration boundary layer (BL) between the barrier exit and the environment (downstream (DS) of the barrier with respect to the diffusion direction). The DS BL was formed by sweeping dry, preheated air across the fabric stack to (1) keep the fabric temperature above the dew point of water and (2) minimize $P_{A,2}$, which was taken as zero (since dry air has no humidity). Before being introduced into the experiment, the sweep gas passed through a commercial moisture trap and filter to remove all water vapor and particulate impurities. The air then entered a heat exchanger with electric heating element whose thermal output was regulated with a Eurotherm 2116 temperature controller operating in PID mode to maintain a set-point temperature. This temperature was measured via bare-bead K-type thermocouple immersed in the flow at the nozzle outlet before the air encountered the experiment. To reduce error arising from fin effect, the thermocouple wire was wrapped around and fixed in good thermal contact with the metal nozzle using Kapton tape. Relative humidity of the sweep gas was measured at 0.9% ± 2.5% using a Comet C4130 digital hygrometer, and the sweep gas remained within ± 0.2 °C of the set-point temperature during all experiments according to the Eurotherm 2116 readout.

The quantity ρ was calculated from the vapor pressure of pure liquid water at the temperature of the liquid water at its air interface inside the chamber. R_{barrier} was determined from Eq. (17) by calculating R_{US} and R_{DS} and by taking $\dot{m}_A$ as the slope of the measured total mass versus time curve in the steady-state and linear regime (see Fig. 5).

An air gap of depth L_{US} between the liquid water–air interface and the fabric barrier prevented liquid water from wicking into the fabric, but it also created a resistance to water vapor mass transfer, R_{US}

$$R_{\text{US}} = \frac{L_{\text{US}}}{D^{\text{US}}_{\text{H}_2\text{O}-\text{Air}}} \tag{18}$$

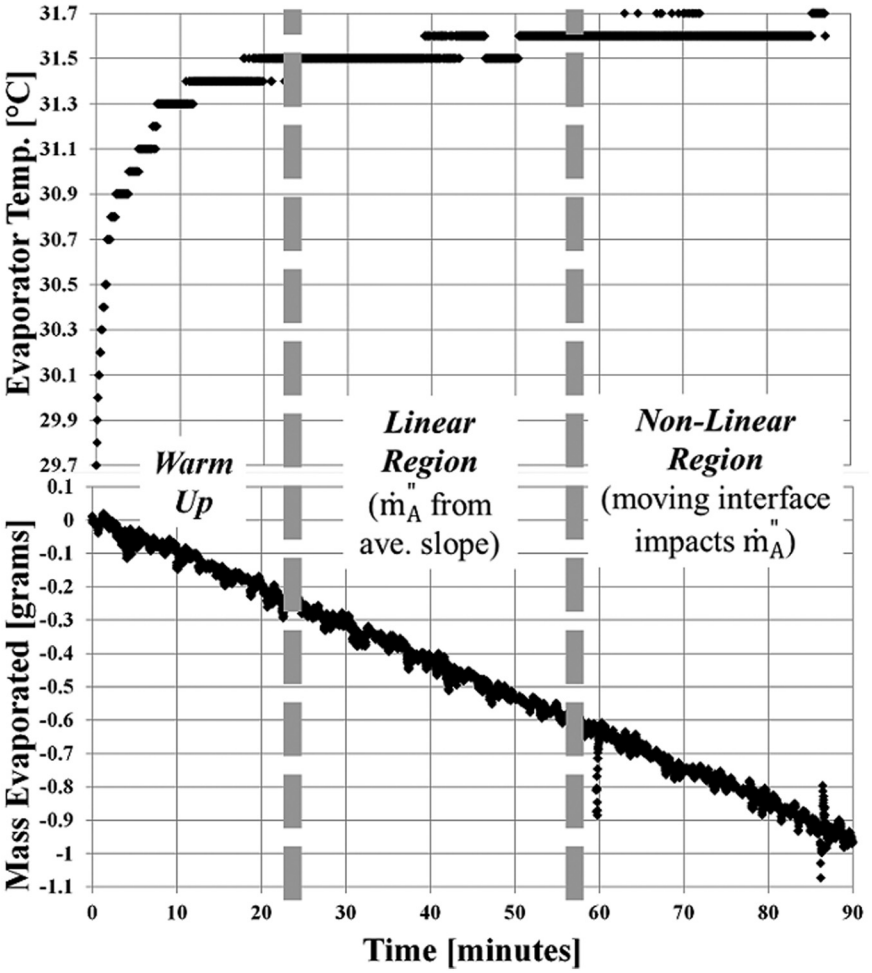

Fig. 5 Raw experimental data for the evaporation chamber temperature (top) and reduction in apparatus mass from water evaporation (bottom) from one characteristic run (two fabric layers). Three regimes are apparent: (1) warm-up, (2) steady temperature with linear mass depletion rate, and (3) steady temperature with nonlinear mass depletion rate. Reported results are averaged data from the first 10 min of the regime of steady temperature with linear mass depletion rate.

where $D^{US}_{H_2O-Air}$ is the molecular diffusivity of water vapor in air [17] at the measured conditions upstream of the barrier (and downstream $D^{DS}_{H_2O-Air}$, Eq. (19)). To prevent the effect of increasing R_{US} owing to liquid water evaporation, $\dot{m}_A$ was analyzed in the early stages of the steady-state temperature period where this curve was linear (see Fig. 5). Thus, L_{US} was treated as constant in Eq. (18).

Tracer measurements and Reynolds number calculations show that the flow of sweep gas (1.0 ± 0.15 m/s, nozzle exit temperatures of 50 °C) created a laminar BL on the DS faces of the barrier and its surrounding flat plate. R_{DS} was calculated from the properties of this BL

$$R_{DS} = \frac{\beta - \alpha}{\overline{Sh_L} D^{DS}_{H_2O-Air}} \tag{19}$$

where α and β, respectively, are the distances from the beginning of the BL (the leading edge of a flat plate) to the two sides of the barrier. $\overline{Sh_L}$ is the average Sherwood Number, Sh, for mass transfer occurring in laminar flow over a horizontal flat plate, estimated by numerically integrating a correlation [17] for the corresponding position-dependent Sh over the barrier diameter, where x is the spatial coordinate parallel to the sweep gas flow, and the momentum BL begins on the flat plate surrounding the barrier, at $x = 0$

$$\overline{Sh_L} = \frac{1}{\beta - \alpha} \int_{\alpha^+}^{\beta} \frac{0.331 Re_x^{\frac{1}{2}} Sc^{\frac{1}{2}}}{\left[1 - \left(\frac{\alpha}{x}\right)^{\frac{3}{4}}\right]^{\frac{1}{3}}} dx, \quad x > a \tag{20}$$

Here, Re_x is the Reynolds number for laminar flow over a flat plate in the x-direction and Sc is the Schmidt Number for dilute water vapor in air. To calculate a practical average mass transport resistance for the mass boundary layer while avoiding a singularity in Eq. (20) at $x = \alpha$, the lower limit of integration was taken at α^+ where $(\alpha^+ - \alpha) = 1$ mm or 2.4% of the barrier diameter.

To set up each experiment, the fabric barrier stack being interrogated was placed atop the brass evaporation chamber. The stack was sealed to the edges of the chamber by a plastic sheet overlay with a cutout slightly larger than the diameter of the dish. Deionized water was injected into the evaporation chamber through a hypodermic tube. At the beginning of each experiment exactly, 3 g of water was pushed into the chamber. Each experimental condition (i.e., the number of fabric layers being interrogated in a stack) was repeated at least three times, and the resulting data analyzed to confirm results were consistent (within experimental uncertainty) for each test.

The temperatures of the evaporation surface (T1), liquid water (T2), fabric US (T3), and fabric DS (T4) were each measured using Omega 5SC-TT-T-40-36 T-type thermocouples (0.076 mm bead outside diameter) connected to an Omega OM-2041 thermocouple reader. Thermocouple T1 was attached to the center of the inside bottom wall of the evaporation chamber with generic rosin core (electrical) solder to provide good thermal contact. The bead of thermocouple T2 remained in the liquid water inside the evaporation chamber unattached to any surface. The beads of thermocouples T3 and T4 were attached to the upstream and downstream faces of the fabric-stack membrane with high thermal-conductivity epoxy.

Mass data and temperature data were taken at 1- and 3-s intervals, respectively. To compare all data streams using the same time index and to eliminate nonphysical data artifacts, a MATLAB code averaged each data stream into 1 min intervals.

Uncertainties denoted by error bars in the figures arise by comprehensively propagating estimated error in measuring barrier porosity, barrier thickness, $\dot{m}_A$, barrier temperature, apparatus temperature, ambient pressure, evaporator geometry, liquid reservoir volume, and sweep gas velocity. Table 1 lists the experimental uncertainties of all measured values.

Table 1 Experimental uncertainties of all measured values. Quantities appearing in regular font are based on manufacturer-stated instrument measurement uncertainties. Quantities appearing in *italics* arise from statistical analyses of at least 20 repeated measurements at a 95% confidence interval.

Measurement	Experimental uncertainty
Apparatus parameters	
Evaporation chamber volume	$\pm 2 \times 10^{-8}$ m^3
Injected water volume	$\pm 2 \times 10^{-8}$ m^3
Evaporation chamber temperature	*±0.2* K
Evaporation rate	*$\pm 1.6 \times 10^{-5}$* g/s
Water heater input power	$\pm 6 \times 10^{-4}$ W
Liquid water temperature	*±0.2* K
Sweep gas velocity	*±0.15* m/s
BL formation distance	$\pm 5 \times 10^{-4}$ m
Fabric properties	
Fabric diameter	$\pm 5 \times 10^{-4}$ m
Fabric thickness	±2.54 μm
Fabric porosity	*±0.01 %*
Upstream fabric temperature	*±0.44* K
Downstream fabric temperature	*±0.88* K
Ambient conditions	
Ambient temperature	*±0.16* K
Ambient RH	*±0.8 %*
Barometric pressure	±500 Pa

Results and Discussion

A representative raw dataset is given in Fig. 5 (in this case two calibration fabric layers were used). Figure 5 shows that measured evaporation chamber temperature increased from room temperature (~29.7 °C) to steady-state temperature (~31.5 °C) as the water is heated. It also shows the associated drop in mass of the apparatus as water evaporated and diffused through the fabric stack. Upon injecting room-temperature water into the apparatus, ~22 min elapsed as the system reached steady-state temperature. Data underpinning reported results were taken during the first 10 min of the ~35-min period where the evaporator was at steady-state temperature and the mass depletion curve slope was linear. As explained above, after ~57 min, enough water evaporated for nonlinearity in the mass depletion curve to be detected owing to the moving liquid–vapor boundary caused by evaporation from the evaporation chamber.

The measured mass transport resistance values, $R_{measured}$, for one, two, three, and four layers of Southern Mills Defender™ 750 fabric are given in Table 2. The measured value for a single layer of fabric, 60.3 ± 14.4 s/m, is consistent with the prescribed result from ASTM F1868 (after the conversion in Eq. (16)), 73.1 ± 7.3 s/m. Moreover, the diffusion coefficient of water vapor in air that results from solving Eq. (10*b*) for $D_{A,B}$ is $(2.02 \pm 0.59) \times 10^{-5}$ m^2/s, which is in agreement with the theoretical value for these conditions, 2.54×10^{-5}. A single layer of fabric imparts no interstitial resistance to mass transport. Therefore, agreement between our gravimetric experiment, the standard ASTM F1868 vapor

Table 2 Experimental and analytical results for water vapor mass transport resistance presented by stacks of calibration fabric of one–four layers

# Layers ( )	$R_{proposed}$ (s/m)	$R_{measured}$ (s/m)	$R_{interstitial}$ (s/m)
1	60.3	60.3 ± 14.4	N/A
2	120.6	155.5 ± 20.4	34.8 ± 20.4
3	181.0	221.5 ± 22.2	20.2 ± 11.1
4	241.3	288.1 ± 26.5	15.5 ± 8.9

transport calibration measurement, and accepted diffusion theory for one layer of fabric validates our gravimetric approach.

Table 2 also contains an $R_{proposed}$ column in which the measured mass transport resistance for a single layer of calibration fabric is multiplied by the number of layers in each stack. The resulting value is analogous to the ASTM F1868 method because it assumes that interstitial mass transport resistance is nonexistent. By subtracting $R_{proposed}$ from $R_{measured}$ and dividing the result by $N-1$ (where N is the total number of fabric layers in the corresponding stack), the interstitial mass transport resistance results. These values are given in the Table 2 column $R_{interstitial}$.

A comparison between $R_{proposed}$ and $R_{measured}$ is plotted in Fig. 6. This plot confirms that stacks of Southern Mills Defender^{TM} 750 calibration fabric of two layers or more present a resistance to mass transport greater than that expected from a simple integral number of layers (in Fig. 6, see the discontinuity in slope for the experimental data at $N=2$). This result contrasts the outcome prescribed in ASTM F1868 and demonstrates the existence of a nontrivial interstitial mass transport resistance, $R_{interstitial}$, when fabrics are layered. Figure 7 shows the measured values for $R_{interstitial}$ resulting from experiments with two, three, and four layers. While the measurement uncertainty in each experiment is of similar magnitude (see Fig. 6), this uncertainty is divided over more interstitial layers as the number of fabric layers increases. So, the interstitial mass transport resistance measurement becomes more precise as the number of layers increases. The average result among the two-, three-, and four-layer experiments is 23.6 s/m, and this value also falls within the experimental uncertainty of all three experimental sets.

The constant slope of mass transport resistance versus number of layers prescribed in ASTM F1868 omits the interstitial mass transport resistances that arise between fabric layers for experiments with two or more fabric layers. Thus, the slope of fabric-stack mass transport resistance versus number of layers in the stack from $0 \le N < 2$ should be less than the slope for $2 \le N \le 4$. In fact, the measured interstitial resistance, 23.6 s/m, is an appreciable fraction (39.1%) of the mass transport resistance presented by a single layer of calibration fabric. This contribution is too large to ignore for purposes of engineering analysis and design.

It is also instructive to apply Eq. (10*b*) to the interstitial mass transport resistance to determine the approximate equivalent air gap thickness. As there is no solid phase in the interstitial space, porosity, ε, is 1. Moreover, while a tortuousity slightly greater than 1 arises from misalignment of pores among adjacent layers, we assume $\tau = 1$ for this analysis. Thus, solving Eq. (10*b*) for the equivalent air gap thickness, L, gives 600 μm.

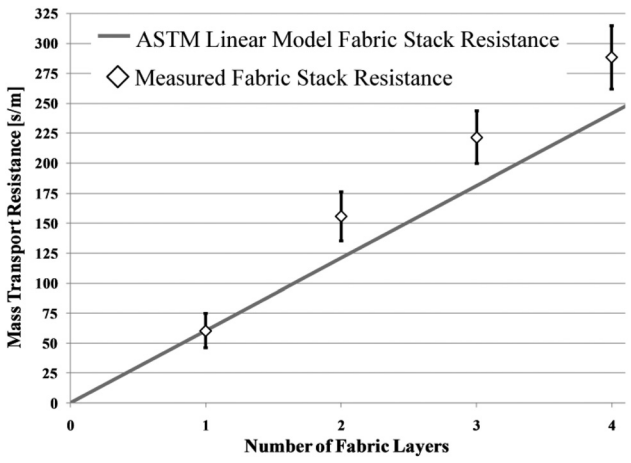

Fig. 6 A comparison of the prescribed ASTM F1868 calibration stack resistance model to measured gravimetric results shows the discontinuity at $N=2$ and subsequent disagreement between prescribed and measured results. This mismatch arises from interstitial mass transport resistances between fabric layers, which are not accounted for in the ASTM F1868 calibration standard.

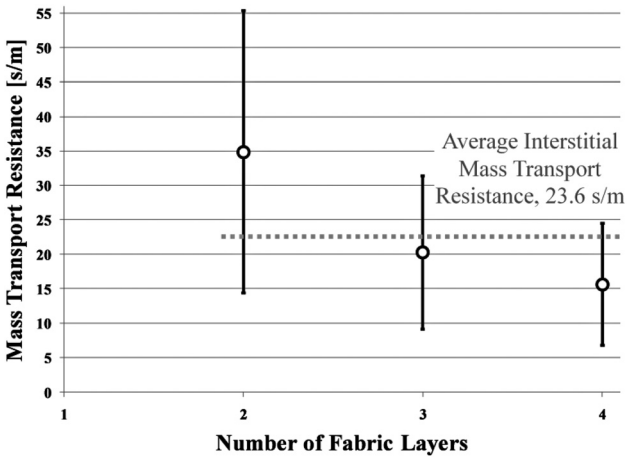

Fig. 7 A constant value of 23.6 s/m agrees with all measurements of interstitial mass transport resistance presented by stacks of calibration fabric with two or more layers

Figure 7 appears to show the beginning of a trend toward an interstitial mass transport resistance asymptotic value near 15 s/m for larger N. It is possible that an asymptotic interstitial mass transport resistance value may emerge as the fabric structure tends toward higher organization, becoming independent of N for large values of N. Certainly, the emergence of new properties arising from large-scale order as three-dimensional objects are created from two-dimensional components has been observed in other layered engineered systems, for example, photonic band gaps in periodic dielectric structures [18].

Data were taken for only two, three, and four layers to enable direct comparison with ASTM F 1868. Examining the underlying experimental uncertainty, a value for interstitial mass transport resistance in the range $14.5 \text{ s/m} < R_{interstitial} < 24.4 \text{ s/m}$ satisfies two-, three-, and four-layer experimental conditions. This range contains the apparent asymptotic value, ~15 s/m, assuming emergent reduction of layer number on interstitial resistance as N increases. However, the range also contains the constant average result, 23.6 s/m, assuming interstitial resistance does not depend on the number of layers. One possibility to explain the apparent asymptotic trend if interstitial resistance is not a function of N is that as additional fabric layers were added to the stack, they had to be stretched more than the previously applied layers to fit over the evaporation chamber. Barrier porosity of higher layers may have been slightly increased by this stretching, lowering the mass transport resistance, and causing the fabric stacks of higher N to present a lower total mass transport resistance (and lower apparent interstitial resistance) than if their uppermost layers had not been slightly stretched to accommodate the experiment. Future experiments using more than four calibration fabric layers are planned to explore the apparent trend toward an asymptotic interstitial resistance value.

Conclusion

Testing mass transport properties of fabrics is critical to human comfort. Four improvements to the prevailing fabric testing methodology, ASTM F1868 Standard Test Method for Thermal and Evaporative Resistance of Clothing Materials Using a Sweating Hot Plate, were suggested and implemented to improve this test: (1) gravimetric mass transport measurement, (2) incorporating Stefan flow into the transport model, (3) accounting correctly for parasitic apparatus mass transport resistances, and (4) recognizing and measuring interstitial layer mass transport resistances.

These improvements were implemented and evaluated by running tests using one, two, three, and four layers of Southern Mills

Defender™ 750 fabric, the calibration standard used for ASTM F1868, using a new gravimetric experimental apparatus configuration. The mass transport resistances of the gravimetric method and ASTM F1868 are related through working-fluid thermodynamic properties, and 17.0 is the numerical ratio of these values for prescribed ASTM 1868F test conditions.

This numerical relationship arises because thermodynamic properties of the working fluid (water) are contained within the ASTM mass transport resistance. Three major drawbacks arise from these embedded working-fluid properties: (1) measured R_{ASTM} values cannot be applied to working fluids other than water; (2) R_{ASTM} is not a pure Ohms Law equivalent mass transport resistance, and it cannot be used for quantitative engineering analysis of mass transport problems; and (3) while the value of R_{ASTM} for calibration fabric is prescribed by a standard, its true experimental value is highly susceptible to variations in working-fluid properties. These drawbacks best suit R_{ASTM} (and the approach used to measure it) as a comparative index between fabric samples that does not provide a numerical mass transport resistance result competent for engineering analysis or design.

Using the gravimetric approach described here, the mass transport resistance for a single layer of calibration fabric was measured. It was 60.3 ± 14.4 s/m, which is consistent with the prescribed result from ASTM F1868 (after multiplying by the conversion factor), 73.1 ± 7.3 s/m. Also, the diffusion coefficient for water vapor in air measured by the experiment, $(2.02 \pm 0.59) \times 10^{-5}$ m^2/s, is in agreement (within experimental uncertainty) with the theoretical value for these conditions, 2.54×10^{-5} m^2/s. Agreement with the existing ASTM approach and with diffusion theory for a condition where no interstitial mass transport resistance is present (e.g., for a single layer of fabric) provides confidence in the validity of the new gravimetric approach.

For stacks of two or more calibration fabric layers, the new gravimetric approach does not agree with the prescribed ASTM F1868 result owing to interstitial mass transport resistances neglected by ASTM F1868. Indeed, for stacks of Southern Mills Defender™ 750 calibration fabric, the measured average interstitial mass transport resistance, 23.6 s/m, is 39.1% the value of a single fabric layer. This interstitial mass transport resistance is too significant to be ignored in proper engineering design of textile systems.

Acknowledgment

This research was sponsored, in part, by the National Science Foundation Research Experiences for Undergraduates (RUE) program (NSF Grant Number EEC-100485) and the Metroplex Research Consortium for Electronic Devices and Materials (MRCEDM). We also gratefully acknowledge the Missions Department of the Egyptian Ministry of Higher Education, which awarded Dr. Aissa the fellowship enabling his participation in this project.

Nomenclature

A = area
BL = boundary layer
$D_{A,B}$ = bulk diffusion coefficient of species A in B
$D^{DS}_{H_2O-Air}$ = downstream diffusion coefficient of water in air
$D^{US}_{H_2O-Air}$ = upstream diffusion coefficient of water in air
L = porous barrier thickness
L_{US} = upstream air gap depth
$\dot{m}_A$ = mass flux of gas species A through a porous barrier
$\dot{m}''_{A,pore}$ = mass flux of A per unit area through a single pore
$\dot{m}_{A,Fick}$ = mass flux calculated via the Fickian diffusion model
$\dot{m}_{A,Stefan}$ = mass flux calculated via the Stefan flow model
N = number of fabric layers
P_i = total pressure at station i
$P_{i,A}$ = partial pressure of species A at station i
$\dot{Q}''$ = heat flux per unit area
R_{ASTM} = mass transport resistance arising from ASTM F1868
$\overline{R}$ = gas constant for water vapor
$R_{barrier}$ = mass transport resistance of a porous barrier
R_{DS} = downstream resistance to mass transport
Re_x = local Reynolds number in the x-direction
R_{Fick} = mass transport resistance arising from Fick's Law
$R_{interstitial}$ = interstitial mass transport resistance
$R_{measured}$ = measured mass transport resistance
$R_{proposed}$ = barrier resistance multiplied by number of layers in the stack
R_{US} = upstream resistance to mass transport
Sc = Schmidt number
Sh = local Sherwood number
$\overline{Sh_L}$ = average Sherwood number
T = temperature
x = spatial coordinate parallel to the sweep gas flow
y_A = mole fraction of species A
$y_{A,i}$ = mole fraction of species A at station i
z = spatial coordinate along the transport direction

Greek Symbols

α = sweep gas mass transport boundary layer beginning
β = sweep gas mass transport boundary layer end
ΔH_{fg} = latent heat of vaporization
ε = porosity
ρ = total concentration (by mass)
$\rho_{A,i}$ = concentration (by mass) of species A at station i
τ = tortuosity

References

[1] ASTM F1868, 2005, "Standard Test Method for Thermal and Evaporative Resistance of Clothing Materials Using a Sweating Hot Plate," *Annual Book of ASTM Standards*, Vol. 11, American Society for Testing and Materials, West Conshohocken, PA.
[2] Huang, J., and Qian, X., 2007, "A New Test Method for Measuring Water Vapour Permeability of Fabrics," Meas. Sci. Technol., **18**(9), pp. 3043–3047.
[3] Gibson, P. W., Kendrick, C., Rivin, D., Sicuranza, L., and Charmchi, M., 1995, "An Automated Water Vapor Diffusion Test Method for Fabrics, Laminates, and Films," J. Ind. Text., **25**, pp. 322–345.
[4] Gibson, P. W., Schreuder-Gibson, H., and Rivin, D., 2001, "Transport Properties of Porous Membranes Based on Electrospun Nanofibers," Colloids Surf., A, **187–188**, pp. 469–481.
[5] Huang, J., 2007, "Review of Test Methods for Measuring Water Vapour Transfer Properties of Fabrics," Cell. Polym., **26**(3), pp. 167–191.
[6] Huang, J., and Qian, X., 2008, "Comparison of Test Methods for Measuring Water Vapor Permeability of Fabrics," Text. Res. J., **78**, pp. 342–352.
[7] McCullough, E. A., Kwon, M., and Shim, H., 2003, "A Comparison of Standard Methods for Measuring Water Vapour Permeability of Fabrics," Meas. Sci. Technol., **14**(8), pp. 1402–1408.
[8] Gibson, P. W., 1993, "Factors Influencing Steady-State Heat and Water Vapour Transfer Measurements for Clothing Materials," Text. Res. J., **63**, pp. 749–764.
[9] Huang, J., 2006, "Sweating Guarded Hot Plate Test Method," Polym. Test., **25**, pp. 709–716.
[10] Traum, M. J., Griffith, P., Thomas, E. L., and Peters, W. A., 2008, "Latent Heat Fluxes Through Soft Materials With Micro-Truss Architectures," ASME J. Heat Transfer, **130**, p. 042403.
[11] Johnson, D. W., Yavuzturk, C., and Pruis, J., 2003, "Analysis of Heat and Mass Transfer Phenomena in Hollow Fiber Membranes Used for Evaporative Cooling," J. Membr. Sci., **227**(1–2), pp. 159–171.
[12] Traum, M. J., Thomas, E. L., and Peters, W. A., 2011, "Effects of Nano to Micro Pore Diameter on Water Vapor Transport Diffusivities Within Porous Polycarbonate Barriers," Nanoscale Microscale Thermophys. Eng., **15**(2), pp. 123–131.
[13] Cussler, E. L., 1997, *Diffusion: Mass Transfer in Fluid Systems*, Cambridge University Press, New York.
[14] Hunter, J. B., and Blass, H., 1944, "Thermodynamic Properties of Aqueous Salt Solutions—Latent Heats of Vaporization and Other Properties by the Gas Current Method," Ind. Eng. Chem., **36**(10), pp. 945–953.
[15] Hernandez, A., Calvo, J. I., Prádanos, P., Palacio, L., Rodríguez, M. L., and de Saja, J. A., 1997, "Surface Structure of Microporous Membranes by Computerized SEM Image Analysis Applied to Anopore Filters," J. Membr. Sci., **137**, pp. 89–97.
[16] Calvo, J. I., Bottino, A., Capannelli, G., and Hernández, A., 2004, "Comparison of Liquid–Liquid Displacement Porosimetry and Scanning Electron Microscopy Image Analysis to Characterize Ultrafiltration Track-Etched Membranes," J. Membr. Sci., **239**, pp. 189–197.
[17] Mills, A. F., 1999, *Basic Heat and Mass Transfer*, 2nd ed., Prentice Hall, Upper Saddler River, NJ.
[18] Ho, K. M., Chan, C. T., Soukoulis, C. M., Biswas, R., and Sigalas, M., 1994, "Photonic Band Gaps in Three Dimensions: New Layer-by-Layer Periodic Structures," Solid State Commun., **98**(5), pp. 412–416.